

ECG-SMART-NET: A Deep Learning Architecture for Precise ECG Diagnosis of Occlusion Myocardial Infarction

Nathan T. Riek, Murat Akcakaya, Zeineb Bouzid, Tanmay Gokhale, Stephanie Helman, Karina Kraevsky-Philips, Rui Qi Ji, Ervin Sejdic, Jessica K. Zègre-Hemsey, Christian Martin-Gill, Clifton W. Callaway, Samir Saba, Salah Al-Zaiti

Abstract— In this paper we describe ECG-SMART-NET for identification of occlusion myocardial infarction (OMI). OMI is a severe form of heart attack characterized by complete blockage of one or more coronary arteries requiring immediate referral for cardiac catheterization to restore blood flow to the heart. Two thirds of OMI cases are difficult to visually identify from a 12-lead electrocardiogram (ECG) and can be potentially fatal if not identified in a timely fashion. Previous works on this topic are scarce, and current state-of-the-art evidence suggests that both random forests with engineered features and convolutional neural networks (CNNs) are promising approaches to improve the ECG detection of OMI. While the ResNet architecture has been successfully adapted for use with ECG recordings, it is not ideally suited to capture informative temporal features within each lead and the spatial concordance or discordance across leads. We propose a clinically informed modification of the ResNet-18 architecture. The model first learns temporal features through temporal convolutional layers with 1xk kernels followed by a spatial convolutional layer, after the residual blocks, with 12x1 kernels to learn spatial features. The new ECG-SMART-NET was benchmarked against the original ResNet-18 and other state-of-the-art models on a multisite real-world clinical dataset that consists of 10,893 ECGs from 7,297 unique patients (rate of OMI = 6.5%). ECG-SMART-NET outperformed other models in the classification of OMI with a test AUC score of 0.889 ± 0.027 and a test average precision score of 0.587 ± 0.087 .

Index Terms— Convolutional Neural Network, Electrocardiogram, Occlusion Myocardial Infarction, Residual Network

I. INTRODUCTION

Deep learning has been widely adopted for applications such as image classification, natural language processing, supply chain, and healthcare

This work was supported in part by the National Institutes of Health under Grant RO1HL137761, the National Center for Advancing Translational Sciences under grant KL2TR0011009, and the National Heart, Lung and Blood Institute under grant T32HL129964 (*Corresponding author: Nathan T. Riek*).

Nathan T. Riek (email: ntr14@pitt.edu), Murat Akcakaya, and Zeineb Bouzid are with the Department of Electrical and Computer Engineering, University of Pittsburgh, Pittsburgh, PA, USA.

Karina Kraevsky-Phillips, Tanmay Gokhale, Christian Martin-Gill, Clifton W. Callaway, and Samir Saba are with the University of Pittsburgh Medical Center (UPMC), Pittsburgh, PA, USA.

Tanmay Gokhale, Samir Saba, and Salah Al-Zaiti are with the Division of Cardiology, University of Pittsburgh, Pittsburgh, PA, USA.

Karina Kraevsky-Phillips, and Salah Al-Zaiti are with the Department of Acute and Tertiary Care Nursing, University of Pittsburgh, Pittsburgh, PA, USA.

diagnostics [1][2][3][4]. Deeper models can learn more complex features in the data, however, when models get too deep, they start to decline in performance due to the vanishing gradient problem [5][6]. To overcome this problem, the ResNet architecture presents the use of skip connections [1]. ResNet was designed primarily for image classification tasks and the original architecture was trained using input images of dimensions 224 x 224 pixels. Since its conception, the ResNet architecture has been modified and used by many researchers for electrocardiogram (ECG) classification tasks [7][8][9]. Since ECGs are multi-channel time series data and not images, the original ResNet-18 architecture requires some architectural adjustments. In this work, we propose a modified ResNet-18 architecture, ECG-SMART-NET, to be used with 12-lead median beat ECGs for binary Occlusion Myocardial Infarction (OMI) classification.

OMI is a potentially fatal condition where blood flow is completely blocked in one or more coronary arteries resulting in acute myocardial infarction (i.e., heart attack). Thus, it is important that OMI is quickly and correctly identified so that patients can receive life-saving reperfusion therapy to restore blood flow through blocked arteries and salvage myocardium. Unlike other heart conditions that can be more readily identified by ECG changes (i.e. ST-elevation myocardial infarction [STEMI]), OMI does not always present obvious patterns on an ECG recording, increasing risk of poor clinical outcomes for these patients from delays in reperfusion therapy [10]. This provides an opportunity for machine learning (ML) models to rapidly identify the less visually obvious ECG patterns linked to OMI.

The current state-of-the-art models for OMI classification are a random forest (RF) with engineered features and a proprietary convolutional neural network (CNN) [11][12]. The benefit of

Stephanie Helman is with the School of Medicine, Department of Medicine, Division of General Internal Medicine, University of Pittsburgh, Pittsburgh, PA, USA.

Christian Martin-Gill, Clifton W. Callaway, and Salah Al-Zaiti are with the Department of Emergency Medicine, University of Pittsburgh, Pittsburgh, PA, USA.

Rui Qi Ji and Ervin Sejdic are with the Edward S. Rogers Department of Electrical and Computer Engineering, University of Toronto, Toronto, Ontario, Canada.

Ervin Sejdic is with the North York General Hospital, Toronto, Ontario, Canada.

Jessica K. Zègre-Hemsey is with the School of Nursing, University of North Carolina (UNC), Chapel Hill, NC, USA.

RFs is that they are easily explainable because they require the researcher to select the features to be used as input [2]. The features can be further interpreted using importance rankings, such as Shapley values. Furthermore, they do not require extremely large datasets to train. The downside of RFs is that they require multiple preprocessing steps to obtain the desired features. For ECG data, this may include filtering, median beat calculation, median beat segmentation, and feature calculation. Additionally, there may be useful information in the ECG that the selected features do not capture. Conversely, CNNs learn their own features automatically through the training process and therefore require fewer preprocessing steps [13]. This often leads to higher performance from CNNs than classical ML models like RFs [14]. The tradeoff is that CNNs require larger datasets to train and are less easily explainable since the model learns its own features.

ML models for ECG must be explainable for four main reasons [15][16]: 1) to justify clinical decisions made by the model; 2) to identify the shortcomings of the model in order to make improvements; 3) to identify new physiological patterns in the data; and 4) for users to understand when to override the decisions of the model.

To overcome the lack of inherent explainability of CNNs, researchers have used saliency maps to identify the most important regions of the input data for the model to make its prediction [17]. Within ECG research, saliency maps have often been used to confirm the clinical relevance of the features identified by CNN models [18][19][20][21][22].

The aim of this work is to design a clinically informed OMI classification model, ECG-SMART-NET, which can compete with the proprietary state-of-the-art CNN while maintaining a high level of clinical explainability. OMI is linked with lead-specific temporal ECG features, including ST segment elevation [23][24]. OMI is also linked to cross-lead spatial ECG information such as reciprocal changes [23][24]. With these OMI features in mind, ECG-SMART-NET used a clinically informed design to first learn lead-specific temporal features followed by cross-lead spatial features. To maintain a high level of clinical explainability, saliency maps were leveraged, identifying the most important leads and within-lead regions for OMI classification. ECG-SMART-NET was compared to other CNN approaches and state-of-the-art RF built using one of the largest prehospital ECG datasets with OMI labels.

II. METHODS

A. Model Architecture

ECG-SMART-NET was based on the ResNet-18 architecture but required modifications. ResNet-18 includes convolutional and MaxPool layers with kernels of dimensions $k \times k$ and was designed for use with images of size 224×224 pixels. However, with 12-lead ECG data, these two-dimensional convolutional layers learn features across leads and time simultaneously. ECG data contains important lead-specific temporal features and cross-lead spatial features. Therefore, the traditional ResNet-18 architecture is not the most appropriate architecture for ECG data.

It is important to first identify ECG components and their relevance to clinical practice before appreciating the architecture modifications that were made. Figure 1 shows the

locations of the P wave, QRS complex, ST segment, and T Wave on a single ECG lead for one heartbeat. Clinically relevant lead-specific temporal features can be calculated within each of these locations. These features, commonly linked to OMI, include ST segment elevation or depression and hyperacute T waves [23][24]. ST segment elevation occurs when the ST segment is above the isoelectric line. The isoelectric line marks no electrical activity. ST segment depression occurs when the ST segment is below the isoelectric line. Hyperacute T waves often have larger amplitudes, are broad-based, and are symmetrical. Hyperacute T waves can be a precursor to ST segment elevation.

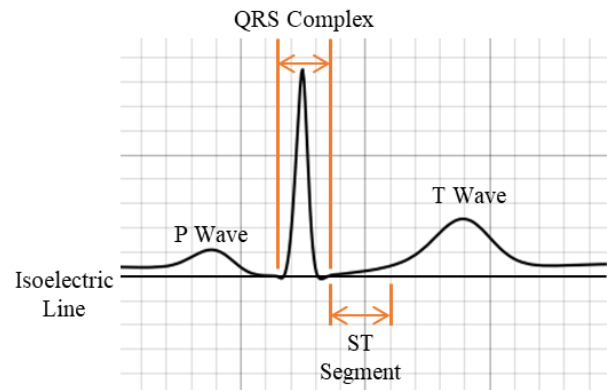


Fig. 1. This is an ECG from a single lead for a single heartbeat. The important segments of this waveform are the P wave, QRS complex, ST segment, and T wave.

In addition to lead-specific temporal features, spatial features are important and are the reason multi-lead ECGs are recorded. Each ECG lead provides a different spatial view of a heartbeat. Figure 2 gives the locations of each of the 12 ECG leads in Cartesian space. Reciprocal changes are important spatial features for the identification of OMI [23][24]. A reciprocal lead is a lead opposite the direction of another lead. For example, lead aVL is a reciprocal lead of lead aVF and if changes are present in lead aVF, we should also look for changes in lead aVL. An example of an important reciprocal change is the presence of ST elevation in some leads, and ST depression in reciprocal leads, indicating potential STEMI.

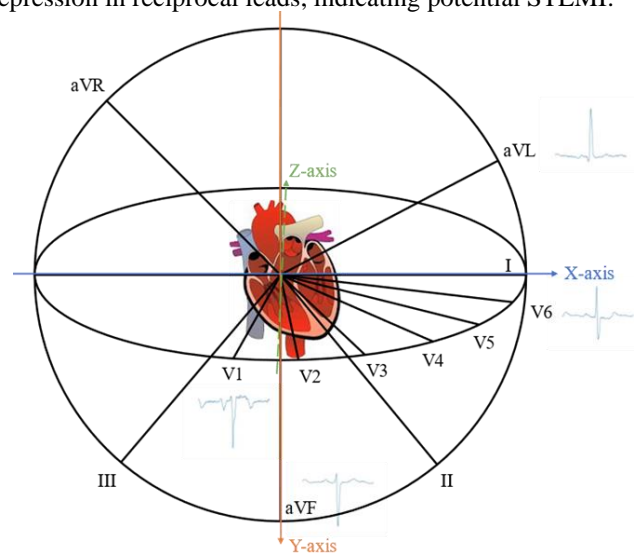


Fig. 2. The Cartesian coordinates for the 12 ECG leads.

Unlike ResNet-18, ECG-SMART-NET first identifies lead-specific temporal features and then learns cross-lead spatial features. Starting with the ResNet-18 architecture, all convolutional and MaxPool layers were modified to have kernels of dimensions $1 \times k$ instead of $k \times k$ (temporal ResNet-18). This allowed the model to learn important temporal features within each lead of the ECG before collapsing across leads. To learn cross-lead spatial information, a spatial convolutional layer was added after the residual blocks with kernels of dimensions 12×1 . Only one spatial convolutional layer was used to keep the model small as ECG data can be difficult to obtain. ECG-SMART-NET is not the first model to incorporate temporal followed by spatial convolution with ECG data. This concept was applied to classification of asymptomatic left ventricular dysfunction (ALVD) by the Mayo Clinic [25]. The ECG-SMART-NET architecture parameters are provided in Tables 1 and 2 for reproducibility. Table 1 gives the overall model architecture parameters and Table 2 provides the parameters for the residual blocks within the model.

TABLE 1
ECG-SMART-NET MODEL ARCHITECTURE

Layer	Output Dimensions	Parameters
Input	1x12x400	-
2D Conv	64x12x200	Kernel: (1,7), Stride: (1,2), Padding: (0,3), Batch Norm, ReLU
MaxPool	64x12x100	Kernel: (1,3), Stride: (1,2), Padding: (0,1)
Residual Block 1	64x12x100	First Stride1: (1, 1)
Residual Block 2	128x12x50	First Stride2: (1, 2)
Residual Block 3	256x12x25	First Stride3: (1, 2)
Residual Block 4	512x12x13	First Stride4: (1, 2)
2D Conv	512x1x13	Kernel: (12,1), Stride: (1,1), Padding: (0,0)
AvgPool	512x1x1	(1,1) global average
Flatten	512	-
Fully Connected	2	(512, 2 classes)

TABLE 2
ECG-SMART-NET RESIDUAL BLOCK

Residual Block	
Layer	Parameters
2D Conv	Kernel: (1,3), Stride: First Stride, Padding: (0,1), Batch Norm, ReLU
2D Conv	Kernel: (1,3), Stride: (1,1), Padding: (0,1), Batch Norm
Shortcut Connection	ReLU
2D Conv	Kernel: (1,3), Stride: (1,1), Padding: (0,1), Batch Norm
2D Conv	Kernel: (1,3), Stride: (1,1), Padding: (0,1), Batch Norm
Shortcut Connection	ReLU

ECG-SMART-NET was compared to the original ResNet-18 model, a temporal ResNet-18 architecture that used $1 \times k$ kernels, the Mayo Clinic ALVD model, and current state-of-the-art RF OMI model. The ResNet-18 model was pretrained on the ImageNet dataset [26]. The first convolutional layer was modified to take in one channel of data instead of 3 and the final fully connected layer was modified to have an output size of 2. Model architectures are provided in Figure 3.

B. Model Tuning

The ECGs were split into ten stratified folds to maintain the same OMI prevalence within the training, validation, and test sets. Patients with multiple ECGs were kept within the same fold to prevent data leakage into the validation and test sets. The models were trained on eight folds, validated on one fold, and tested on one fold. This process was repeated ten times, each time using different folds as the validation and test sets, so that each fold was validated and tested on only once. The models were trained for 100 epochs with a batch size of 128. To handle class imbalance, within each batch of training data, the majority class (no OMI) was randomly undersampled so that there was a 1:1 ratio of both classes, giving the model the chance to learn to identify the rare positive class. This method was implemented so new combinations of the majority class would be seen in each epoch. The models utilized a cross entropy loss and Adam optimizer with an initial learning rate of $1e-5$ (the initial learning rate for the Mayo Clinic ALVD model was adjusted to $1e-4$ to improve performance). Initial learning rate was optimized for all architectures by selecting the initial learning rate that achieved the highest average validation score in Equation 1. A learning rate scheduler was used with a patience of 3 and a multiplication factor of 0.8. The scheduler decreased the learning rate if the validation score in Equation 1 did not increase within 3 epochs. AUC is the area under the receiver operating characteristics (ROC) curve and AP is the average precision across the precision recall curve. Alpha was set to $2/3$. The model at the epoch with the highest validation score was saved for each fold to prevent the model from overfitting to the training dataset. A combination of AUC and AP was used so that the selected model would consider the tradeoff between sensitivity and specificity, as well as between precision and sensitivity. After training, the models were evaluated on the test sets. This results in 10 trained models for each architecture (one model for each split of folds). The models were trained using PyTorch v2.0.1 and Python v3.11.3 in the Visual Studio Code Editor. The computer runs on the Windows 10 operating system with an Intel Xeon E5-2650 CPU, NVIDIA TITAN Xp GPU, and 128 GB RAM.

$$(\alpha)AUC_{val} + (1 - \alpha)AP_{val} \quad (1)$$

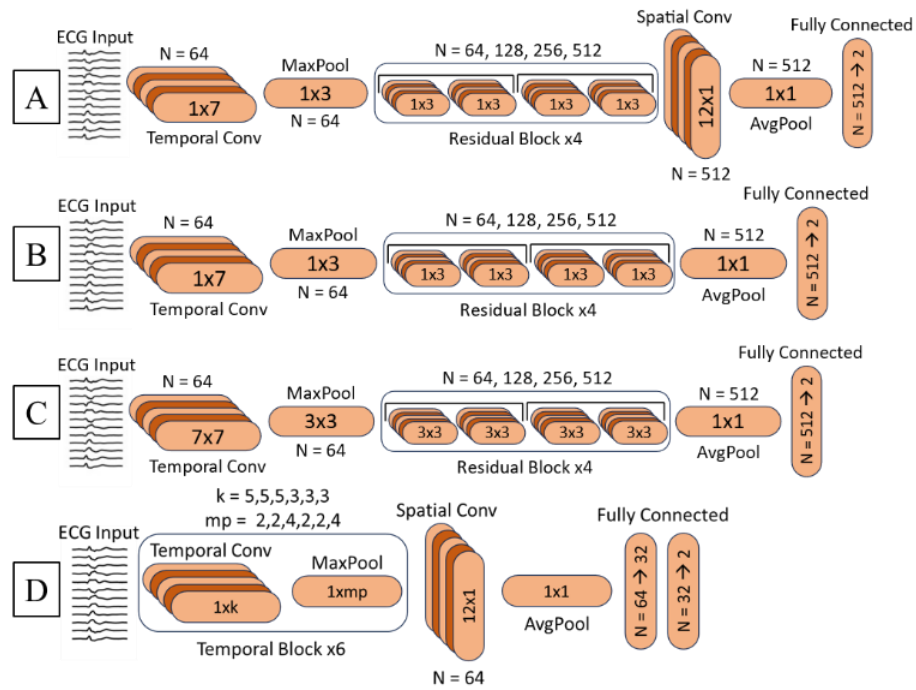


Fig. 3. Model Architectures: A) ECG-SMART-NET, B) Temporal ResNet-18, C) ResNet-18, D) Mayo Clinic ALVD Model.

C. Saliency Maps

ECG-SMART-NET was trained on 10 different data splits resulting in 10 different models. The model with the highest test score (best generalizability) from Equation 1 was selected for further analysis with saliency maps. Saliency maps highlight the most informative regions of a model’s input in reaching an outcome prediction. This can add significant explainability to a CNN. Saliency maps were generated using the Saliency class in the Captum library for Python. The Saliency class provides the absolute value of the gradients with respect to inputs for a target outcome class. A saliency map was calculated for all 83 positive OMI cases within the test set of the selected model. Lead contributions were calculated by taking the sum of the saliency values within each lead and dividing by the total sum of saliency values across all leads. The saliency maps were then averaged within 40 millisecond windows, corresponding to one small square on ECG graph paper. The saliency maps were then mapped to a color scale ranging from bright yellow (low importance) to dark red (high importance). Lastly, the 83 saliency maps were normalized within each lead separately and were averaged together to give one aggregate saliency map.

D. Dataset

The dataset in this study consisted of prehospital 12-lead median beat ECGs from patients with a primary complaint of non-traumatic chest pain. The median beat ECG is a median of all beats from the original 10-second recording (500 s/s, 0.05-150 Hz). An example of both the 10-second and median beat ECGs are shown in Figure 4.

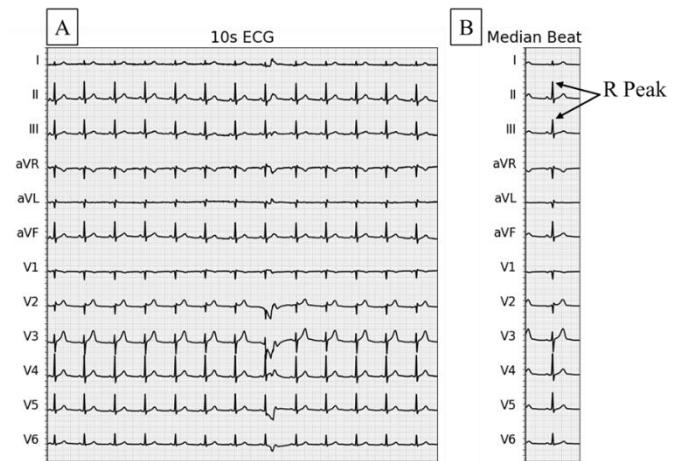


Fig. 4. (A) A raw 12-lead 10-second prehospital ECG recording. (B) The median beat ECG from the same recording, centered at the R Peak. Median beats were found by filtering the 10-second ECG, detecting beats centered at R peaks, removing ectopic beats, and taking the median of the remaining beats.

Data were collected from hospital systems within two different US cities (Pittsburgh, PA and Charlotte, NC). A total of 10,893 ECGs from 7,297 unique patients were recorded with OMI labels. OMI labels were created using angiographically defined culprit lesions [11]. The Pittsburgh patient cohort was 47% female with an average age of 59 and 6.3% OMI prevalence and the Charlotte patient cohort was 44% female with an average age of 60 and 6.8% OMI prevalence. Across the two sites, the patient cohort was 46% female with an average age of 60 and 6.5% OMI prevalence. The dataset is summarized in Table 3.

TABLE 3
DATASET DESCRIPTION

City	ECGs	Patients	Age	Sex (Female)	OMI
Pittsburgh	5088	4127	59 (± 16)	1937 (47%)	261 (6.3%)
Charlotte	5805	3170	60 (± 15)	1400 (44%)	217 (6.8%)
Total	10893	7297	60 (± 16)	3337 (46%)	478 (6.6%)

The median beats have dimensions 12 leads x 600 datapoints sampled at 500 samples per second. Median beats were centered at the R Peak as shown in Figure 4. Before training any models, the median beats were shortened by removing the first 150 and last 50 points from each lead resulting in dimensions 12 leads x 400 datapoints. Lastly, the data were z-score normalized within each lead separately.

III. RESULTS

A. Average Model Performance

All neural networks were trained for 100 epochs on each of the 10 data partitions, saving the model within the 100 epochs with the highest validation score for testing. Figure 5 provides the average validation curves for AUC, AP, cross-entropy loss, and the score function presented in Equation 1. The clouds around each of the average validation curves span ± 1 standard deviation. ECG-SMART-NET on average took 20 epochs to reach the maximum validation score.

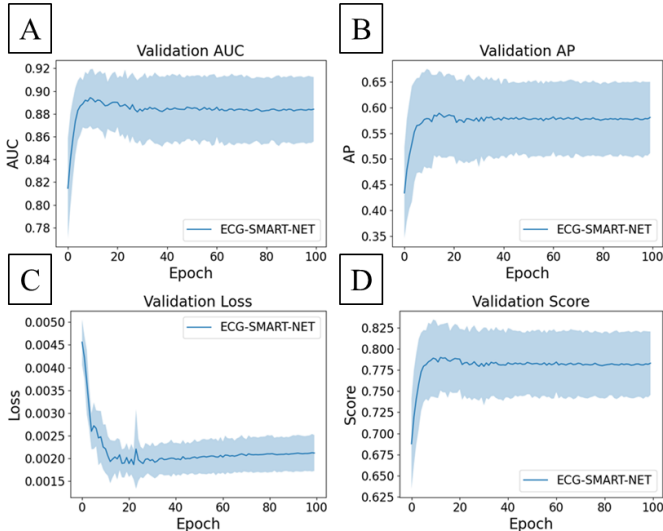


Fig. 5. Average validation curves: A) AUC, B) Average precision score (AP), C) Cross-entropy loss, D) $2/3$ AUC + $1/3$ AP.

Table 4 shows the average performance for each of the models across the 10 folds for both the validation and test partitions. ECG-SMART-NET achieved the highest average validation and test metrics. The Mayo Clinic ALVD model was the second-best model for all validation and test metrics. The temporal ResNet-18 performed the third best for all metrics except test AP. The RF achieved higher validation and test AUC scores than the ResNet-18 model, but lower validation and test AP scores.

TABLE 4
MODEL PERFORMANCE COMPARISON

Model	Val AUC	Val AP	Test AUC	Test AP
ECG-SMART-NET	0.902 ± 0.025	0.605 ± 0.085	0.889 ± 0.027	0.587 ± 0.087
Mayo Clinic ALVD model	0.886 ± 0.020	0.584 ± 0.057	0.877 ± 0.032	0.566 ± 0.106
Temporal ResNet-18	0.884 ± 0.024	0.565 ± 0.093	0.871 ± 0.023	0.532 ± 0.077
ResNet-18 (pretrained on ImageNet)	0.858 ± 0.033	0.544 ± 0.084	0.857 ± 0.033	0.537 ± 0.087
Random Forest	0.872 ± 0.023	0.516 ± 0.077	0.864 ± 0.026	0.514 ± 0.082

B. Selected Model Performance

To gain further insights into ECG-SMART-NET, one of the 10 saved models was selected for further analysis. The model with the best generalization to the test set (highest test score using Equation 1) was kept. This model achieved a validation AUC of 0.917, validation AP of 0.598, a test AUC of 0.930, and a test AP of 0.691. The train, validation, and test splits contained 8691 ECGs (772 OMI), 1117 ECGs (101 OMI), and 1085 ECGs (83 OMI), respectively. Figure 6 provides the ROC and Precision-Recall curves. The model performed slightly better for the test set compared to the validation set.

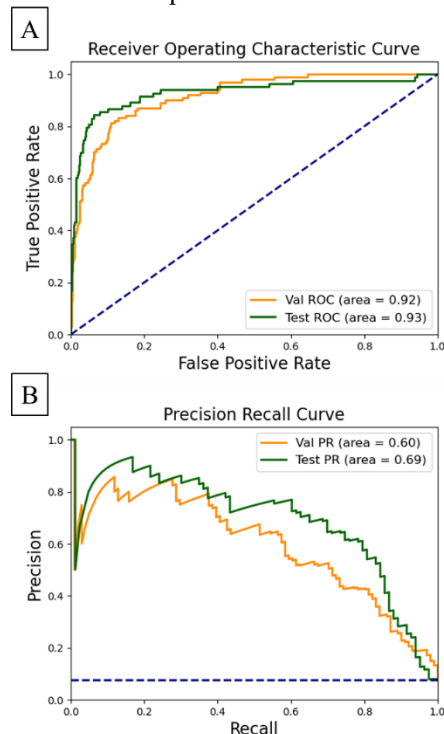


Fig. 6. Selected model performance: A) ROC curve, B) Precision-Recall curve.

An operating point of 0.57 was selected by maximizing the F1 score on the validation set. The model achieved an F1 score of 0.603 on the validation set and 0.681 on the test set. Table 5 provides accuracy, sensitivity, specificity, positive predictive value, negative predictive value, F1 score, AUC, and AP on the validation and test sets.

TABLE 5

SELECTED MODEL PERFORMANCE METRICS

	Acc	Sens	Spec	PPV	NPV	F1	AUC	AP
Val	0.933	0.564	0.969	0.648	0.957	0.603	0.917	0.598
Test	0.947	0.747	0.963	0.626	0.979	0.681	0.930	0.691

C. Saliency Map

The aggregate saliency map across all 83 positive OMI cases in the test set is provided in Figure 7. This figure gives insight into the temporal regions that most commonly help the model identify OMI. These regions, denoted by dark red, appear to occur within the ST segment and T wave for most leads. Furthermore, the aggregate saliency map shows that lead aVL and lead I contribute most frequently to the classification of OMI in this specific dataset. It is important to note that saliency maps for individual ECGs show localized patterns of highest salience, so not all leads, nor the same group of leads, are important for every ECG.

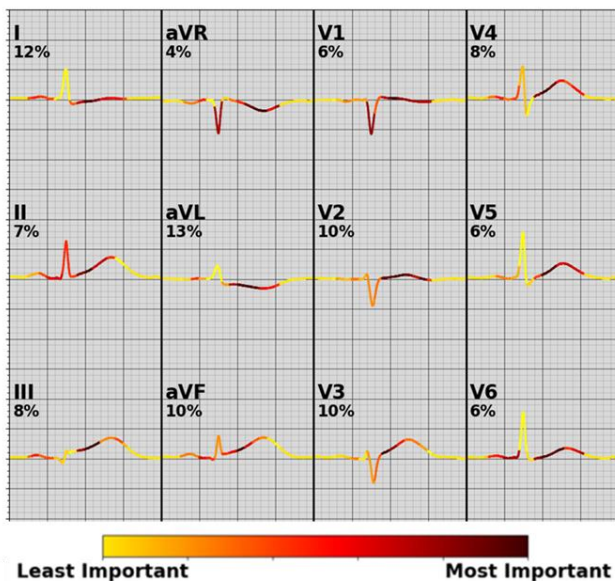


Fig. 7. Average saliency map for 83 OMI cases in test set.

IV. DISCUSSION

ECG-SMART-NET outperformed the standard ResNet-18 architecture, Mayo Clinic ALVD model, ECG-SMART-NET without spatial convolution, and state-of-the-art RF. The Mayo Clinic ALVD model performed second best compared to all the other models. Both ECG-SMART-NET and the Mayo Clinic ALVD model leverage the use of temporal convolution followed by spatial convolution. Superior model performance indicates that this ordering of layers provides a performance boost for ECG classification tasks. This makes sense clinically because clinicians identify temporal features within each of the ECG leads separately, and also search for reciprocal changes across ECG leads. While both ECG-SMART-NET and the Mayo Clinic ALVD models mimic this clinical practice, there is an architectural difference between the two. ECG-SMART-NET used a residual network architecture while the Mayo Clinic ALVD model was a shallower CNN without skip connections. This resulted in ECG-SMART-NET and Mayo Clinic ALVD models having 19 and 9 layers, respectively. The

deeper architecture allowed ECG-SMART-NET to learn more complex features, which may explain ECG-SMART-NET's better performance.

The state-of-the-art CNN for OMI detection achieved a test AUC of 0.938, accuracy of 90.9%, sensitivity of 80.6%, and specificity of 93.7% on a different dataset [12]. ECG-SMART-NET achieved a test AUC of 0.930, accuracy of 94.7%, sensitivity of 74.7%, and specificity of 96.3%. Both models achieve similar performance. However, the OMI prevalence in their dataset was 21.6%, while the OMI prevalence in our dataset was 6.5%, thus both models should be trained on a common dataset in the future for a fairer comparison. Unfortunately, the state-of-the-art model could not be replicated in this study as the model architecture is proprietary.

ECG-SMART-NET outperforms the state-of-the-art RF model and, with the use of saliency maps, can overcome concerns of explainability. Saliency maps allowed identification of the most important temporal features within each lead and the most important leads for OMI prediction for the selected test set of ECGs. The average saliency map showed that the most informative regions within each lead were the ST segment and T wave. This aligns with current literature suggesting that OMI can be identified from ST elevation, reciprocal ST depression, T wave inversion, and hyperacute T waves [23][24]. The average saliency map also showed that lead aVL and lead I were the most informative for OMI classification. This could be caused by the coronary distribution of OMI in the selected test set and may vary for different datasets. This should be investigated further. Saliency maps enhance the explainability of ECG-SMART-NET, which is necessary for eventual clinical adoption.

We have demonstrated that ECG-SMART-NET can identify OMI better than a traditional ResNet-18 and the current state-of-the-art RF. Furthermore, we demonstrated the value of applying temporal convolutional layers followed by spatial convolutional layers for deep learning approaches with 12-lead ECG data. With saliency maps, we can add explainability to ECG-SMART-NET to identify the most informative leads and regions within lead for OMI classification. Other multichannel biosignals, including electroencephalograms (EEG) or electromyograms (EMG), may benefit from ECG-SMART-NET for classification tasks due to its ability to learn both channel-specific temporal features and spatial features across channels.

Clinical implications for this work include enhanced identification of OMI using the 12-lead ECG. 12-lead ECG changes beyond ST segment elevation are not as visually obvious to clinicians in many cases. Leveraging explainable ML models that include the use of color-coded saliency maps will support objective, data driven, and timely decision support during moments of diagnostic uncertainty.

REFERENCES

- [1] K. He, X. Zhang, S. Ren, and J. Sun, "Deep residual learning for image recognition," in *CVPR*, 2016, pp. 770-778.
- [2] G. Baryannis, S. Dani, and G. Antoniou, "predicting supply chain risks using machine learning: the trade-off between performance and

- interpretability,” *Future Generation Computer Systems*, vol. 101, pp. 993-1004, Dec. 2019, doi: 10.1016/j.future.2019.07.059.
- [3] D. Khurana, A. Koli, K. Khatter, and S. Singh, “Natural language processing: state of the art, current trends and challenges,” *Multimedia tools and applications*, vol. 82, no. 3, pp. 3713-3744, Jan. 2023, doi: 10.1007/s11042-022-13428-4.
- [4] S. Somani, et al., “Deep learning and the electrocardiogram: review of the current state-of-the-art,” *EP Europace*, vol. 23, no. 8, pp. 1179-1191, Feb. 2021, doi: 10.1093/europace/uaa377.
- [5] M. Roodschild, J.G. Sardinas, and A. Will, “A new approach for the vanishing gradient problem on sigmoid activation,” *Progress in Artificial Intelligence*, vol. 9, pp. 351-360, Oct. 2020, doi: 10.1007/s13748-020-00218-y.
- [6] S. Hochreiter, “The vanishing gradient problem during learning recurrent neural nets and problem solutions,” *International Journal of Uncertainty, Fuzziness and Knowledge-Based Systems*, vol. 6, no. 2, pp. 107-116, Apr. 1998, doi: 10.1142/S0218488598000094.
- [7] M. Cao, et al., “ECG heartbeat classification using deep transfer learning with convolutional neural network and STFT technique,” *Journal of Physics: Conference Series*, vol. 2547, 2023, doi: 10.1088/1742-6596/2547/1/012031.
- [8] E. Jing, et al., “ECG heartbeat classification based on an improved ResNet-18 model,” *Computational and Mathematical Methods in Medicine*, May 2021, doi: 10.1155/2021/6649970.
- [9] N. Nonaka and J. Seita, “In-depth benchmarking of deep neural network architectures for ECG diagnosis,” in *PMLR*, 2021, vol. 149, pp. 414-439.
- [10] D. Tziakas, G. Chalikias, R. Al-Lamee, and J.C. Kaski, “Total coronary occlusion in non ST elevation myocardial infarction: time to change our practice?,” *International Journal of Cardiology*, vol. 329, pp. 1-8, Apr. 2021, doi: 10.1016/j.ijcard.2020.12.082.
- [11] S.S. Al-Zaiti, et al., “Machine learning of ECG diagnosis and risk stratification of occlusion myocardial infarction,” *Nature Medicine*, vol. 29, no. 7, pp. 1804-1813, Jun. 2023, doi: 10.1038/s41591-023-02396-3.
- [12] R. Herman, et al., “International evaluation of an artificial intelligence-powered electrocardiogram model detecting acute coronary occlusion myocardial infarction,” *European Heart Journal-Digital Health*, vol. 5, no. 2, pp. 123-133, Nov. 2023, doi: 10.1093/ehjdh/ztd074.
- [13] R. Mahajan, R. Kamaleswaran, and O. Akbilgic, “Comparative analysis between convolutional neural network learned and engineered features: a case study on cardiac arrhythmia detection,” *Cardiovascular Digital Health Journal*, vol. 1, no. 1, pp. 37-44, Jul. 2020, doi: 10.1016/j.cvdhj.2020.04.001.
- [14] M.S. Roodposhti, J. Aryal, A. Lucieer, and B.A. Bryan, “Uncertainty assessment of hyperspectral image classification: deep learning vs random forest,” *Entropy*, vol. 21, no.1, pp. 78, Jan. 2019, doi: 10.3390/e21010078.
- [15] S.S. Al-Zaiti and R.R. Bond, “Explainable-by-design: challenges, pitfalls, and opportunities for the clinical adoption of AI-enabled ECG,” *Journal of Electrocardiology*, vol. 81, pp. 292-294, Nov. 2023, doi: 10.1016/j.jelectrocard.2023.08.006.
- [16] A. Adadi and M. Berrada, “Peeking inside the black-box: a survey on explainable artificial intelligence (XAI),” *IEEE access*, vol. 6, pp. 52138-52160, Sep. 2018, doi: 10.1109/ACCESS.2018.2870052.
- [17] K. Simonyan, A. Vedaldi, and A. Zisserman, “Deep inside convolutional neural networks: visualising image classification models and saliency maps,” in *ICLR*, Apr. 2014, doi: arXiv:1312.6034.
- [18] K.C. Siontis, et al., “Saliency maps provide insights into artificial intelligence-based electrocardiography models for detecting hypertrophic cardiomyopathy,” *Journal of Electrocardiology*, vol. 81, pp. 286-291, Nov. 2023, doi: 10.1016/j.jelectrocard.2023.07.002.
- [19] Y. Jones, F. Deligianni and J. Dalton, “Improving ECG Classification Interpretability using Saliency Maps,” 2020 IEEE 20th International Conference on Bioinformatics and Bioengineering (BIBE), Cincinnati, OH, USA, 2020, pp. 675-682, doi: 10.1109/BIBE50027.2020.00114.
- [20] S. Vijayarangan, et al., “Interpreting Deep Neural Networks for Single-Lead ECG Arrhythmia Classification,” 2020 42nd Annual International Conference of the IEEE Engineering in Medicine & Biology Society (EMBC), Montreal, QC, Canada, 2020, pp. 300-303, doi: 10.1109/EMBC44109.2020.9176396.
- [21] A.M. Storas, et al., “Usefulness of heat map explanations for deep-learning-based electrocardiogram analysis,” *Diagnostics*, vol. 13, no. 14, pp: 2345, Jul. 2023, doi: 10.3390/diagnostics13142345.
- [22] S.A. Hicks, et al., “Explaining deep neural networks for knowledge discovery in electrocardiogram analysis,” *Scientific reports*, vol. 11, no. 1, pp: 10949, May 2021, doi: 10.1038/s41598-021-90285-5.
- [23] H.P. Meyers, et al., “Accuracy of OMI ECG findings versus STEMI criteria for diagnosis of acute coronary occlusion myocardial infarction,” *IJC Heart & Vasculature*, vol. 33, Apr. 2021, doi: 10.1016/j.ijcha.2021.100767.
- [24] D.F. Miranda, et al., “New insights into the use of the 12-lead electrocardiogram for diagnosing acute myocardial infarction in the emergency department,” *Canadian Journal of Cardiology*, vol. 34, no.2, pp: 132-145, Feb. 2018, doi: 10.1016/j.cjca.2017.11.011.
- [25] Z.I. Attia, et al., “Screening for cardiac contractile dysfunction using an artificial intelligence-enabled electrocardiogram,” *Nature Medicine*, vol. 25, no. 1, pp. 70-74, Jan. 2019, doi: 10.1038/s41591-018-0240-2.
- [26] J. Deng, W. Dong, R. Socher, L. -J. Li, Kai Li and Li Fei-Fei, “ImageNet: A large-scale hierarchical image database,” 2009 IEEE Conference on Computer Vision and Pattern Recognition, Miami, FL, USA, 2009, pp. 248-255, doi: 10.1109/CVPR.2009.5206848.